AΦNE TECHNICAL NOTE

NFN - LNF, Accelerator Division

Frascati, May 21, 1997

Note: **MM-25**

THE "LONG" DIPOLES OF THE DAΦNE MAIN RING ACHROMATS

B. Bolli, N. Ganlin, F. Iungo, F. Losciale, M. Paris,
M. Preger, C. Sanelli, F. Sardone, F. Sgamma, M. Troiani

1. Introduction

The first Parallel End Long (PEL in the following) and Sector-like Long (SLL in the following) Dipoles of the Main Rings achromats, built by ANSALDO Energia, were delivered to LNF on October 17, 1996 and January 15, 1997 respectively.

Strictly speaking, these dipoles were not real prototypes, since the only difference with respect to the "short" ones [1] is the total length of the lamination stack. For this reason, less measurements have been performed on these magnets, and we report them in this paper, together with the design parameters, in order to have an easily reachable and complete documentation on all the magnets in the DAΦNE accelerator complex. The magnets have been measured in a random sequence, and the results of magnetic measurements described in this note refer to Serial#4 both for the PEL and SLL magnets.

The main design and measured parameters of the two kinds of dipole are given in Table I. The nominal current (266.2A), as explained in [2], corresponds to a beam energy of 511.8 MeV.

Table I - Long dipoles parameters

	units	PEL (Serial#4)	SLL (Serial#4)
Energy	MeV	511.8	511.8
Nominal current	A	266.2	266.2
Nominal field	T	1.219	1.219
Measured field at magnet center (B_o)	T	1.230	1.214
Deflection Angle	deg	49.5	49.5
Maximum current	A	652.55	652.36
Max. measured field	T	1.839	1.828
Field integral on nominal trajectory	T.m	1.4756	1.4776
Field integral on particle trajectory	T.m	1.4751	1.4746
Magnetic Length (Design)	m	1.21	1.21
Measured length $\int(B/B_o)*dl$	m	1.200	1.217
Magnet gap	mm	75.6	75.6
Turns per pole		144	144
Copper Conductor	mm*mm	12*12	12*12
Cooling Hole Diameter	mm	7	7

2. Electrical and thermal measurements

The resistance of the main coils and backleg coils of the PEL and SLL dipoles was measured by means of a micro-ohm-meter (AOIP mod. OM 20) at room temperature (23°C).

The measured values were:

	Main Coils [mΩ]	Backleg Coil[mΩ]
PEL Dipole	167.5	872.0
SLL Dipole	159.6	949.8

The same measurements were accomplished using the Volt-Ampere method and the following data were measured:

PEL Dipole	Main Coils	44.5 V @ 266.2 A	corresponding to 167.2 mΩ
SLL Dipole	Main Coils	42.2 V @ 266.2 A	corresponding to 158.5 mΩ

The inductance and resistance of the magnets were also measured by means of a LCR meter (LCR meter HP 4284 A) at different frequencies. The results are shown in figures 2.1 and 2.2. The corresponding dc values may be extrapolated from these data. They are consistent with the measured ones, given above.

The magnets were also thermally characterized at the nominal and maximum currents corresponding at beam energies of 510 and ≈750 MeV. Figures 2.3 and 2.4 show the worst thermal values for the PEL and SLL dipole respectively.

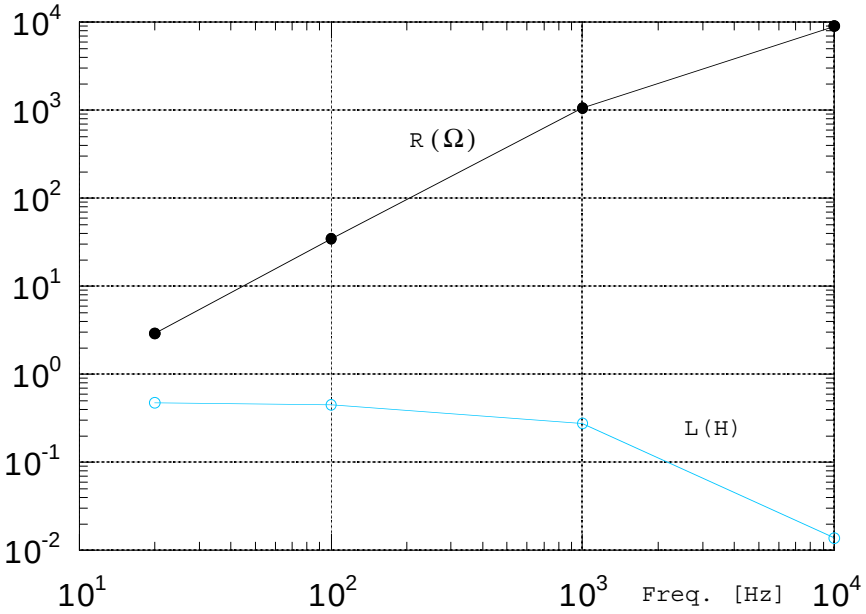

Figure 2.1 - Resistance and inductance versus frequency of the PEL dipole main coils.

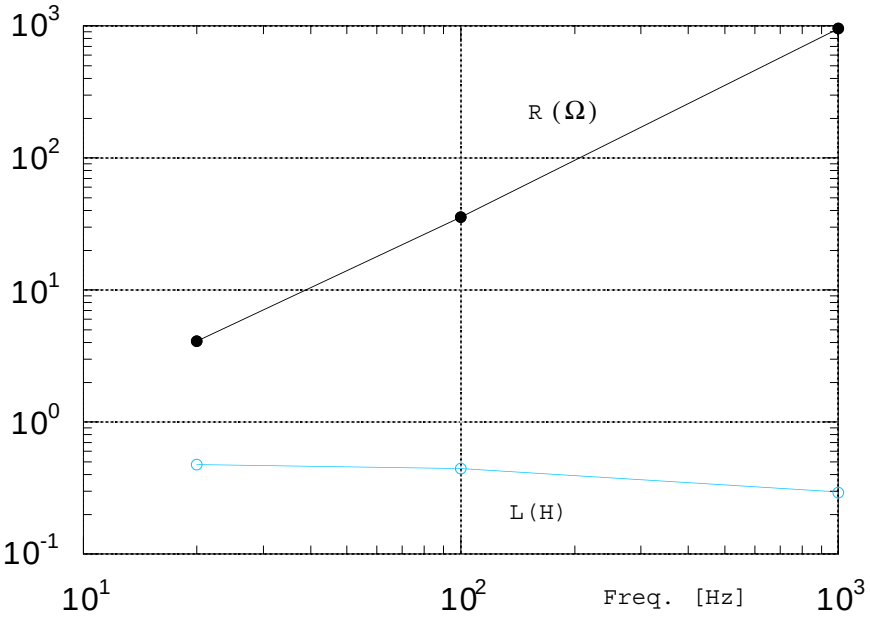

Figure 2.2 - Resistance and inductance versus frequency of the SLL dipole main coils.

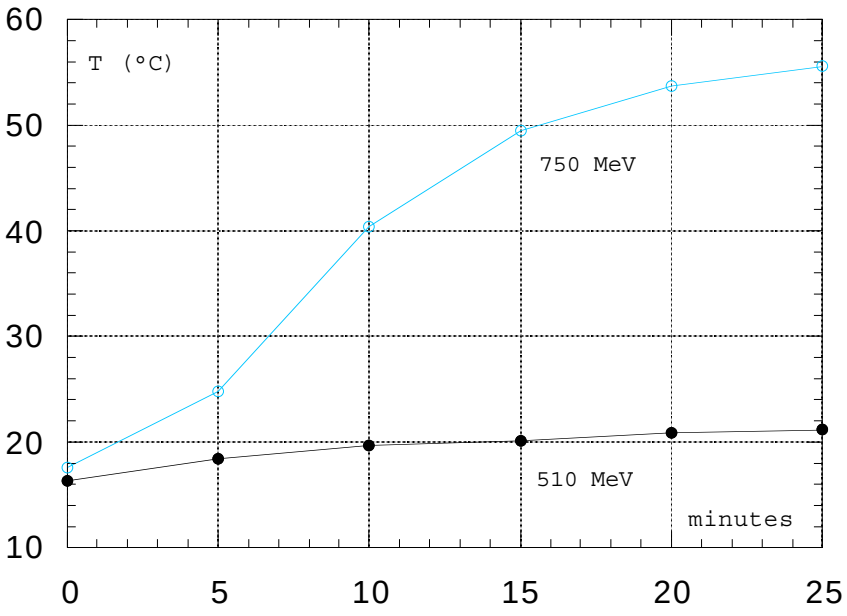

Figure 2.3 - Outlet water temperature increase versus time for the PEL dipole.

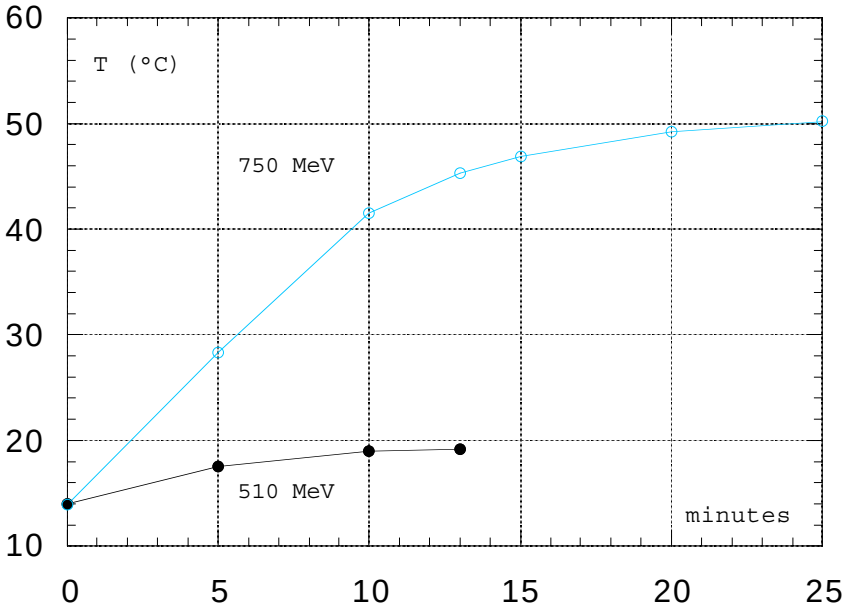

Figure 2.4 - Outlet water temperature increase versus time for the SLL dipole.

3. Magnetic measurements

3.1 - Optimization of the steel length

The magnetic length and the shim shape have been optimized following the procedure adopted for the DAΦNE Accumulator dipoles [3]. In the present case, being the Main Ring magnets of the "C" type, the measurements were easier, since it was not necessary to rotate the dipoles in order to perform the complete scan of the field. The magnets were positioned with their symmetry axis perpendicular to the 2.5 m long "longitudinal" movement of the Hall probe positioning system. The 1m "transverse" movement parallel to the magnet symmetry axis covers easily the required good field region. However, due to the absence of field clamps, the magnets exhibit rather long field tails outside the end caps, especially at the maximum excitation current, so that in some cases it was not possible to extend the measurement at a distance where the field could be defined as negligible (see Section 3.5).

As already observed in the "short" dipole prototypes [1], the field at the magnet center changes slightly as a function of the overall steel length. Figure 3.1 shows the result of the excitation curve of the vertical field component at the magnet center, measured on the SLL dipole in its final configuration. The nominal operating point for the magnet, corresponding to 0.51 GeV beam energy is just at the separation point between the linear and saturation regions.

Following the experience gained on the "short " prototypes, the optimization of the steel length has been performed in a smaller number of steps. Let us remind that in the case of short magnets, where the fringing field region is in the same order of the steel length, it is not correct to simply define the magnetic length as the field integral along the nominal beam trajectory divided by the field value at the magnet center. Actually, the particles are deflected towards the inside of the machine by the fringing field well before the nominal dipole edge, and follow therefore a trajectory displaced from the nominal one by a non negligible amount. The steel length is determined by the condition that, being the 4 types of dipoles powered in series, the field integral on the real trajectory followed by the particles must be the same for all the "long" dipoles, and in the proportion of the nominal deflecting angles with respect to the "short" dipoles [1]. This field integral corresponds to a particle energy of 511.8 MeV at the nominal excitation current of 266.2A.

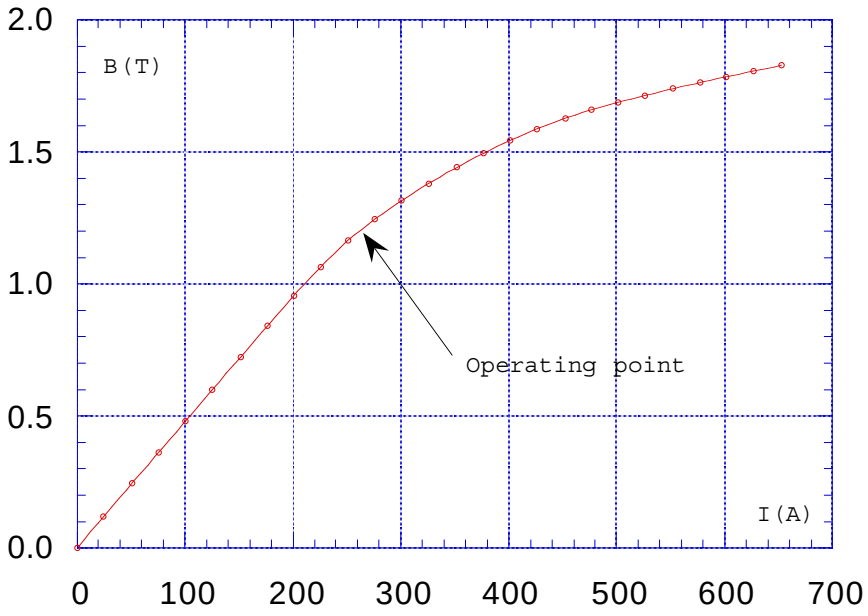

Figure 3.1 - Vertical component of the field at magnet center versus current (SLL Dipole).

We have therefore measured the field along the nominal trajectory, namely a circular sector with the nominal bending radius (1.40056 m) and angle (49.5°) plus two straight lines tangent to the sector at its end points. The same longitudinal scan has been performed along 8 other trajectories, parallel to the first one, in such a way that for each measured point on the nominal trajectory there are other 8 measured points along a line perpendicular to the nominal trajectory at the same longitudinal position. The points were measured in steps of 10 mm along the longitudinal direction on the nominal trajectory and in steps of 10 mm as well in the transverse one, so that the mesh of measured field values extends by ±40 mm in the transverse direction. By interpolating the measurements in this mesh, it is possible to integrate the equations of motion of the particles and find the real trajectory followed by the beam, which depends on the steel length of the magnet. It is assumed that the particles start from the nominal trajectory, a straight line tangent to the nominal bending arc; the energy of the particles is varied until the bending angle is exactly the nominal bending one; of course in this case the output trajectory is a straight line at the nominal bending angle from the input one, but there may be an offset from the ideal output line, due to any possible asymmetry of the field with respect to the symmetry axis of the magnet.

We have also checked that the result does not depend on the number of points used for the transverse fit: being the trajectory of the particles always well below a distance of 10 mm from the nominal one, the field integral found with 9 points is the same as that calculated with the central scan and the two nearby ones.

The PEL Dipole has been measured in its original configuration, and then each removable end cap has been machined to reduce its thickness a first time by 15 mm, a second one by 20 mm, and finally by 25 mm. In addition, the magnet has been measured also without end caps (the original thickness was 31 mm). Figure 3.2 shows the particle energy corresponding to the nominal deflection (49.5°) versus the cut thickness. The linearity is excellent, as already observed for the short dipoles [1].

Figure 3.3 shows the distance between the real and nominal trajectories calculated from the corresponding field maps. All measurements were performed at the same excitation current (266.2 A) in the magnet coil. It can be observed from this figure that this distance decreases when the total steel length is shortened.

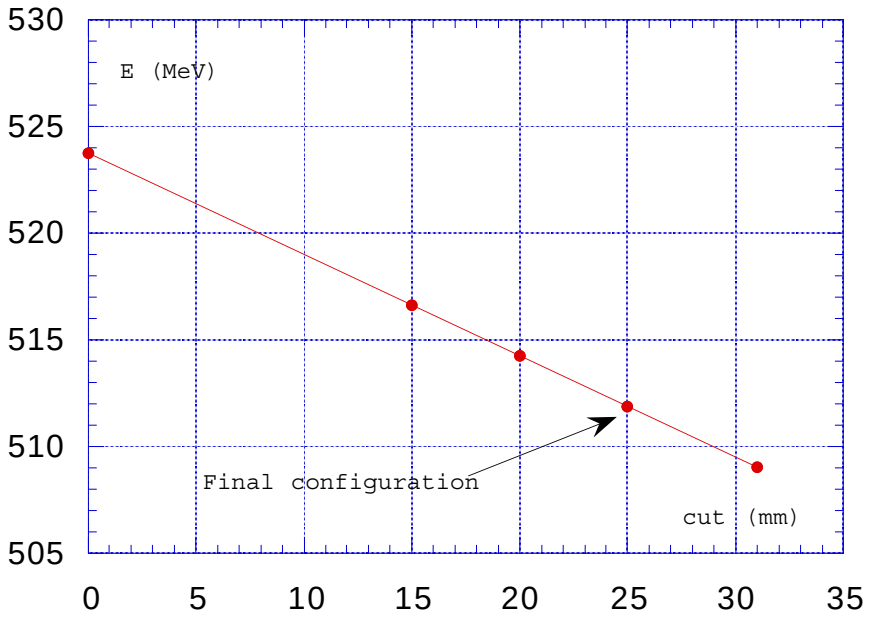

Figure 3.2 - Particle energy for the nominal deflection versus cut thickness.

Due to the linearity in the cut thickness demonstrated by Fig. 3.2, the procedure adopted for the SLL dipole has been straightforward. The magnet was measured in its original configuration and with the end caps removed. Interpolating linearly between the two energies calculated from these two maps, a cut thickness of 8.5 mm was found to match the correct beam energy.

Figure 3.4 gives the ratio of the measured field at the magnet center to the nominal field at the corresponding energy as a function of the cut thickness.

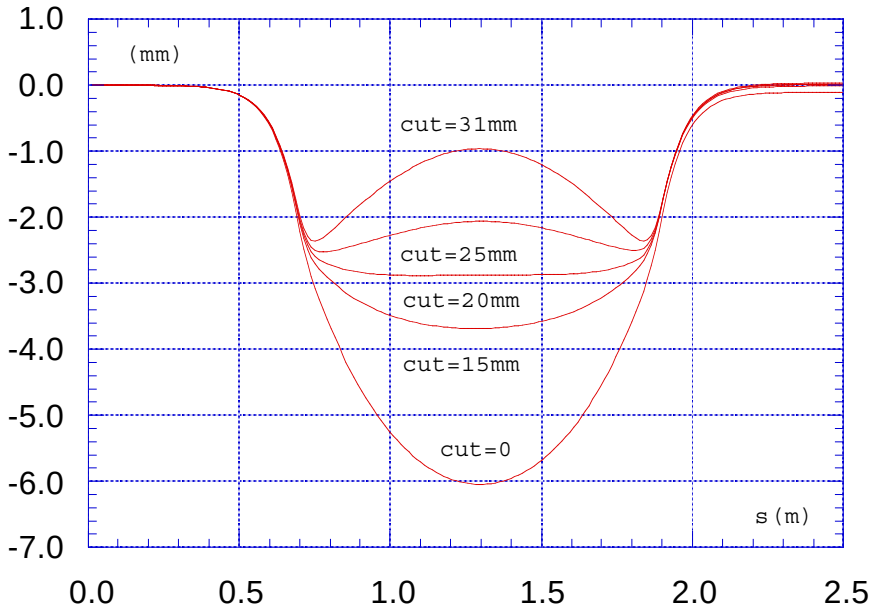

Figure 3.3 - Distance between real and nominal trajectories in the PEL dipole for different depths of the cut performed on the removable end caps.

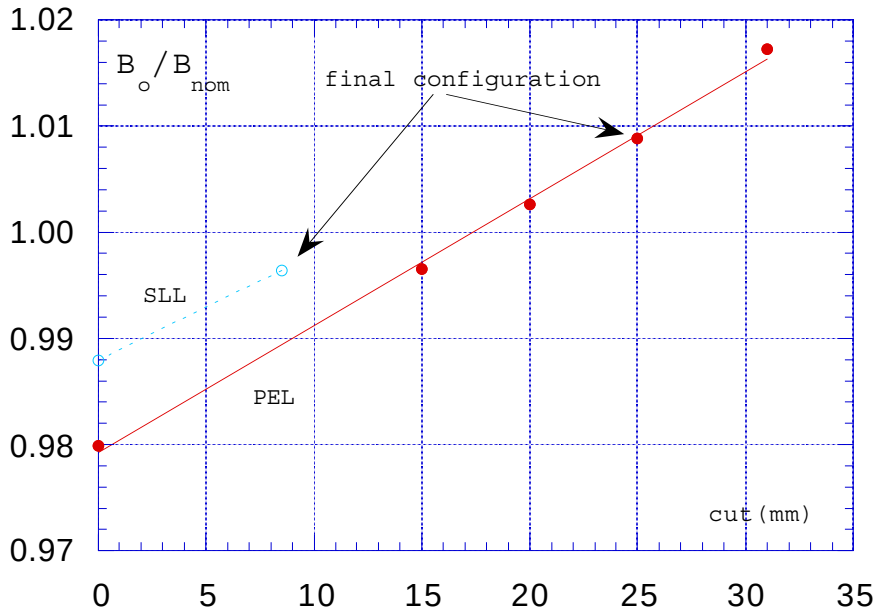

Figure 3.4 - Measured field at the magnet center divided by the nominal field corresponding to the particle energy versus cut thickness.

An unwanted consequence of the displacement between the real and nominal trajectories in the dipole is the overall shortening of the particle orbit, which affects the nominal revolution frequency of the ring. This effect is in any case rather small with respect to the tuning range of the RF cavities. However, it may affect the conditions under which it is possible to obtain the required synchronization between the Accumulator and the Main Rings [3]. The results from the Accumulator commissioning indicate that the machine acceptance is sufficient to compensate for this small mismatch. Figure 3.5 shows the shortening of the trajectory as a function of the cut depth. As already shown in Figure 3.3 this effect is reduced when the total iron length is decreased.

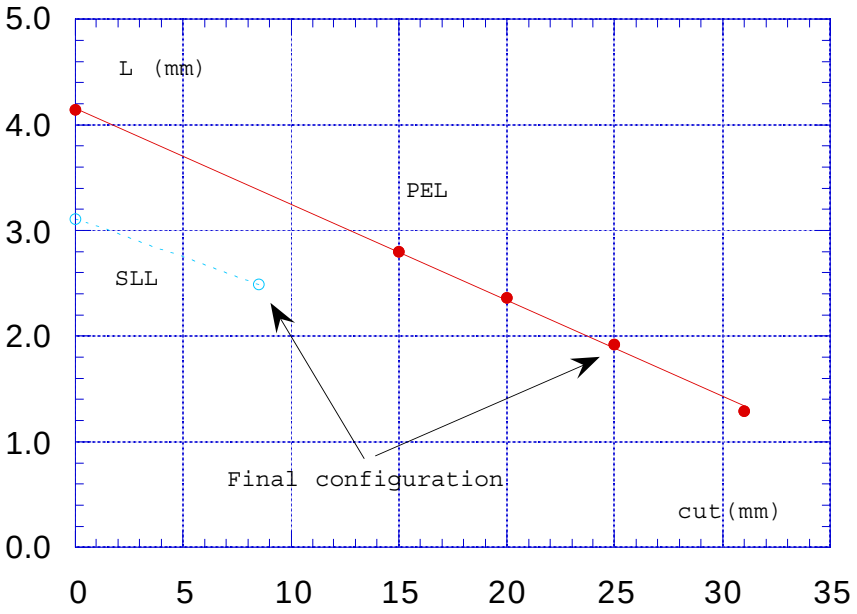

Figure 3.5 - Shortening of the beam trajectory length with respect to the nominal one versus cut thickness.

Figure 3.6 shows the distance between the calculated trajectory and the one for the two dipoles in their final configuration: as already observed in the case of the short dipoles [1], this distance is larger in the SLL magnet.

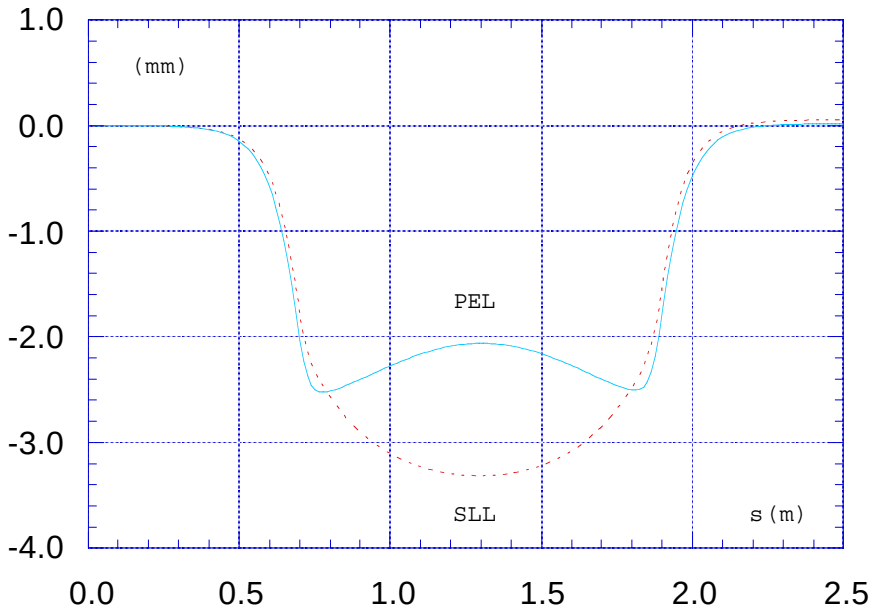

Figure 3.6 - Displacement between real and nominal trajectories in the dipoles in their final configuration (full line = PEL dipole, dotted line = SLL dipole).

3.2 - Optimization of the sextupole contribution

It has been shown in [1] that the fringing field region of short magnets can be seriously affected by sextupole-like contributions. Since this effect depends only on the geometry of the end caps, we have adopted the same design of the short dipoles end caps, leaving the shim thickness as a free parameter. In the case of the PEL dipole we tried first with a shim thickness of 5 mm, and the integrated second order term of the transverse fit was reduced from -0.93 T/m to -0.13 T/m. We decided to increase the shim thickness to 5.5 mm, and the final result for the integrated second order term was -.04 T/m. Extrapolating from the result of the sector short prototype, a thickness larger than that applied to the parallel ends magnet was expected. When the end cap thickness was reduced to match the field integral, the outer side (see Figure 3.6 in Ref.[1]) was not machined, thus realizing a shim of the same thickness of the cut depth. The integrated second order term of the transverse fit for the SLL dipole was reduced from -1.03 T/m with no shim to -0.13 T/m with the shim thickness of 8.5 mm. A further reduction of the integrated second order term would have therefore required the construction of an additional thin iron shim (as in the case of the Accumulator dipole [3]), and it was therefore decided to accept this small residual sextupolar contribution.

Figure 3.7 plots the second order term of the transverse expansion for the two dipoles with the original end caps without shims. It appears that for the PEL dipole there are two peaks of opposite sign in each fringe, while for the SLL magnet the peaks are small and negative, just as observed in the case of the short prototypes. There is no significant sextupole contribution inside the magnets, due to the large width of the poles. Figure 3.8 shows the situation in the final configuration of the shims (5.5 mm for PEL, 8.5 mm for SLL).

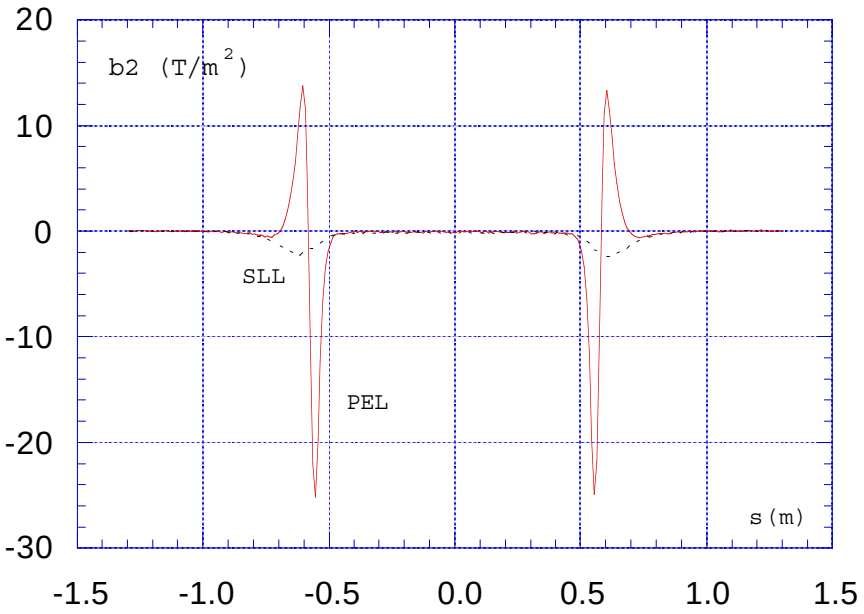

Figure 3.7 - Second order term of the transverse fit versus longitudinal position without shims (full line = PEL dipole, dotted line = SLL dipole).

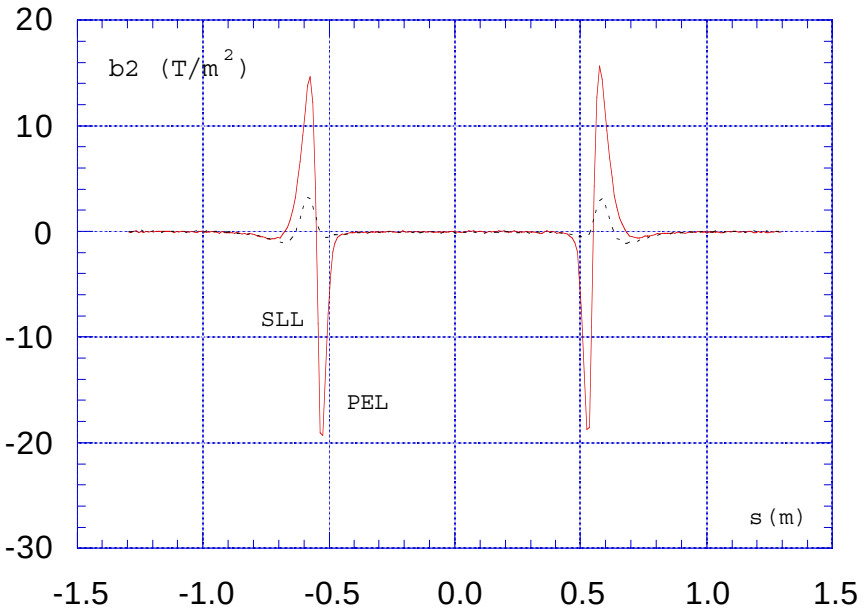

Figure 3.8 - Second order term of the transverse fit versus longitudinal position in the final shim configuration (full line = PEL dipole, dotted line = SLL dipole).

3.3 - Other terms of the transverse expansion in the final configuration.

Figure 3.9 shows the zero order term of the transverse expansion, namely the field value on the nominal trajectory at the nominal working point for the two dipoles. At constant field integral (as explained before), a slight difference between the two fields can be observed: the sector like magnet, as expected, has a flatter field under the poles and a slightly steeper fringe.

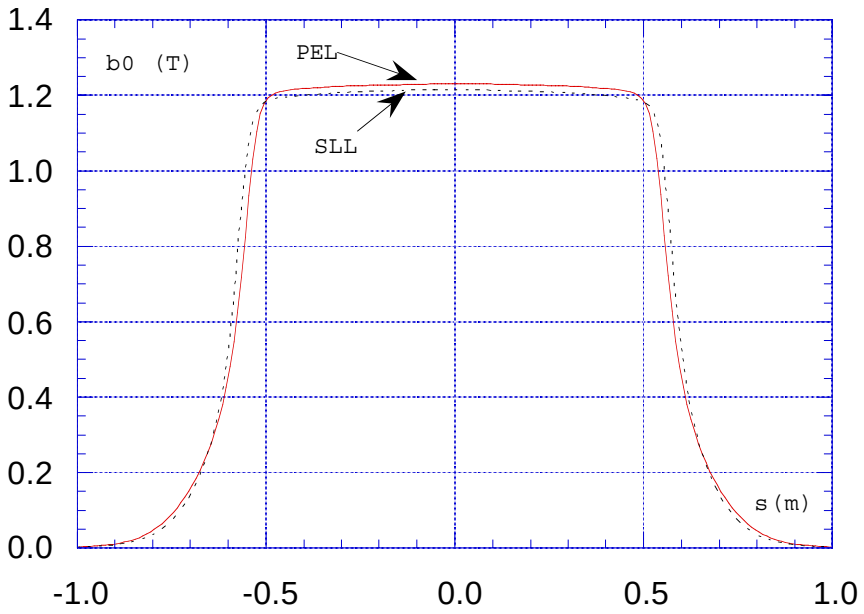

Figure 3.9 - Zero order term of transverse fit (full line = PEL, dotted line = SLL).

The first order term, the point-to-point value of the gradient, is shown in Fig. 3.10. The parallel end magnet has two large negative peaks in the fringing region. Its integrated value of -0.96 T is smaller than the corresponding theoretical value for an ideal magnet with parallel ends (-1.05 T). Part of the difference can be attributed to an effect coming from the fact that the magnet yoke is shorter than the nominal magnetic length, while the angle between the opposite end caps is the nominal one. This introduces a small quadrupole-like contribution of the opposite sign: this happens, as it can be observed in the same figure, also for the sector like magnet, where the integrated quadrupole contribution is 0.01 T.

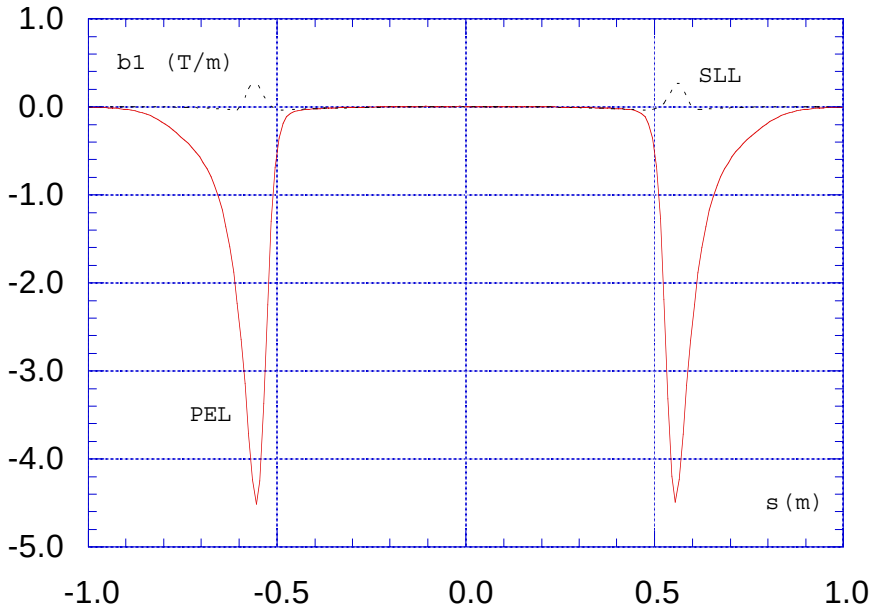

Figure 3.10 - First order term of transverse fit (full line = PEL, dotted line = SLL).

Figures 3.11 and 3.12 show, respectively, the third and fourth order terms of the transverse expansion. As expected, there is a non negligible octupole term in the PEL dipole fringing field, coming from the distortion of the linear term. However, the integrated octupole term (≈9 T/m^2) is still quite small, and should not create harmful effects on the beam dynamics. The fourth order term is almost the same for the two dipoles, one order of magnitude smaller than in the case of the Accumulator one [3].

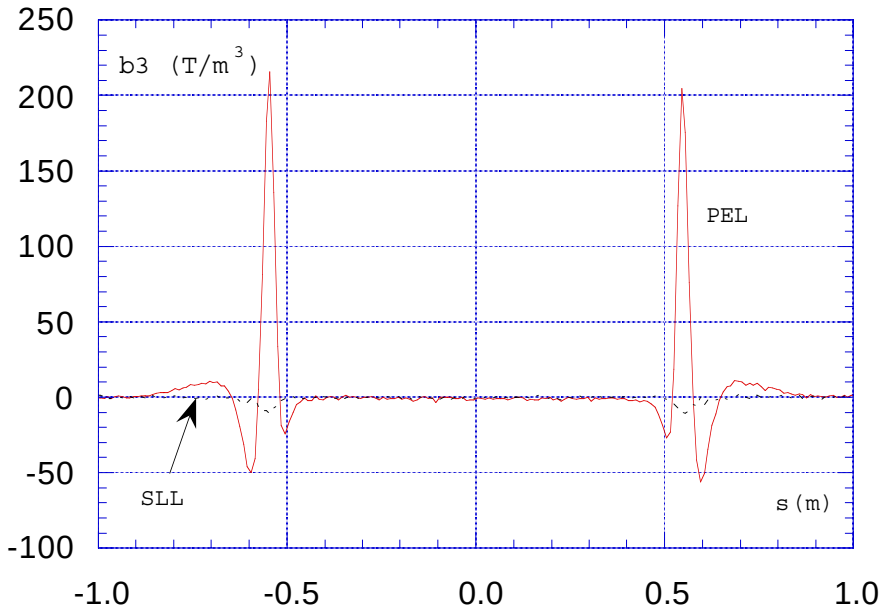

Figure 3.11 - Third order term of transverse fit (full line = PEL, dotted line = SLL).

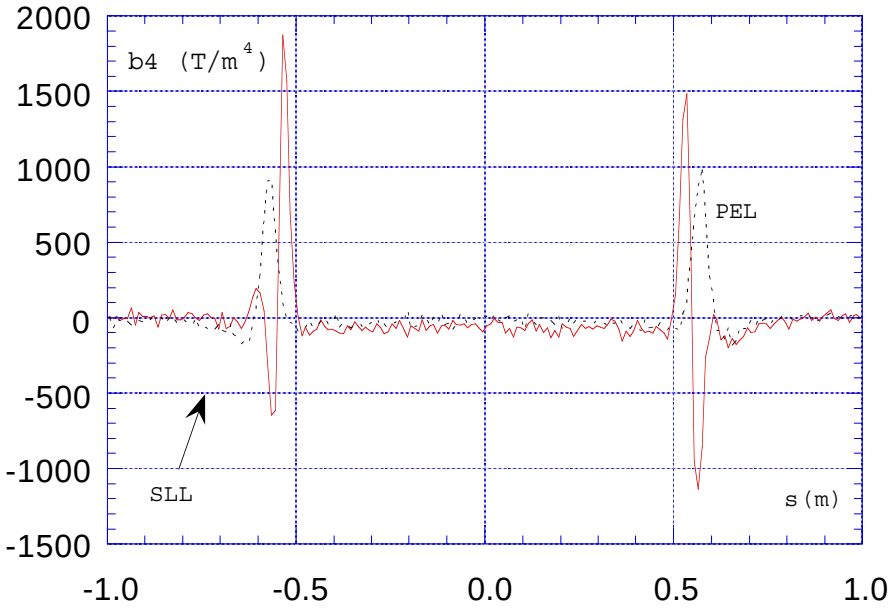

Figure 3.12 - Fourth order term of transverse fit (full line = PEL, dotted line = SLL).

3.4 - Dependence on the excitation current

Both magnets, as explained in this Section, have been optimized at the nominal operation energy of DAΦNE (0.51 GeV per beam), with the steel length determined by the condition of making the field integrals on the real trajectory the same. The main characteristics of the field have been investigated for the SLL dipole also at three different excitation currents, roughly corresponding to beam energies of 0.45, 0.55 and 0.7 GeV. Table II shows the comparison with the Sector-like short dipole [1]

Table II - Beam energy versus excitation current

Current (A)	E_{SLL} (MeV)	E_{SLS} (MeV)	$\Delta E_{SLL-SLS}$	$\Delta E_{backleg}$SLL/SLS
225.4	451.11	452.35	-1.24	±4.2/±4.3
266.2	511.70	511.87	-0.17	±3.1/±2.6
301.0	552.98	552.54	0.44	±2.5/±2.0
502.9	698.30	693.75	4.55	±0.8/±0.8

The maximum difference between the two dipoles has been found at the highest measured current of ≈500A. Each dipole is equipped with a backleg coil powered by a bipolar supply capable of delivering ±10A. The field value at the magnet center has been measured on each magnet at all the above mentioned excitation currents as a function of the current in the winding. The energy change introduced by the correction winding depends on the current in the main coil, due to the saturation shown in Fig. 3.1, and is listed in the last column of the Table: it can be noticed that the energy difference between the two magnets can be compensated at the three lower energies near the nominal operating point of the collider, but not at the last point near 0.7 GeV.

Figure 3.13 shows the ratio between the field measured at the magnet center and the nominal field at the corresponding energy, fitted with a second order polynomial. For sake of simplicity, we plot all the following results of magnetic measurements versus the beam energy corresponding to each excitation current. The full dot corresponds to the value measured for the PEL dipole at the nominal operating point.

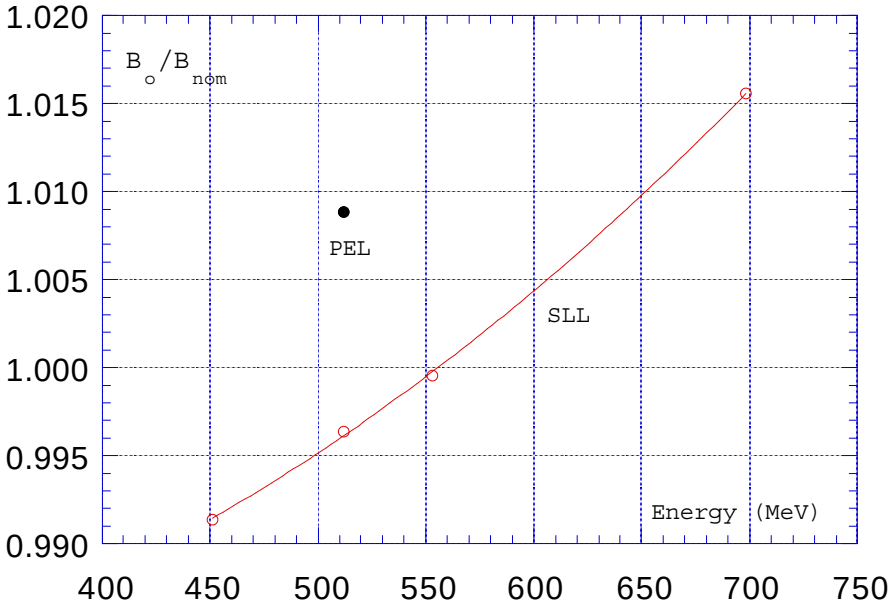

Figure 3.13 - Field at magnet center divided by nominal field versus energy.

The integrated first order term of the transverse expansion is given in Fig. 3.14. The small contribution in the fringing field, described in the preceding subsection, decreases slightly at high currents.

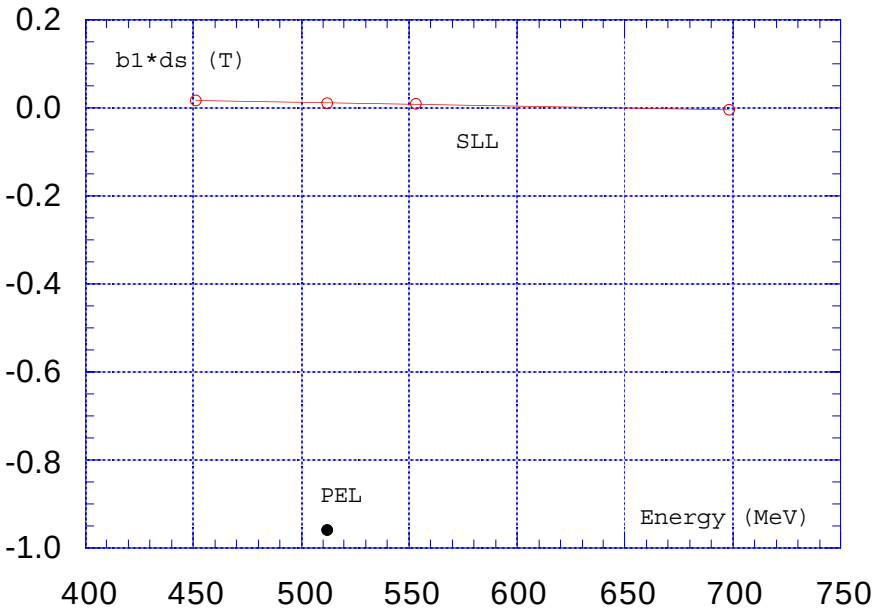

Figure 3.14 - Integrated first order term of the transverse fit versus energy.

Figures 3.15, 3.16 and 3.17 show the corresponding behaviours for the second, third and fourth order terms of the transverse fit.

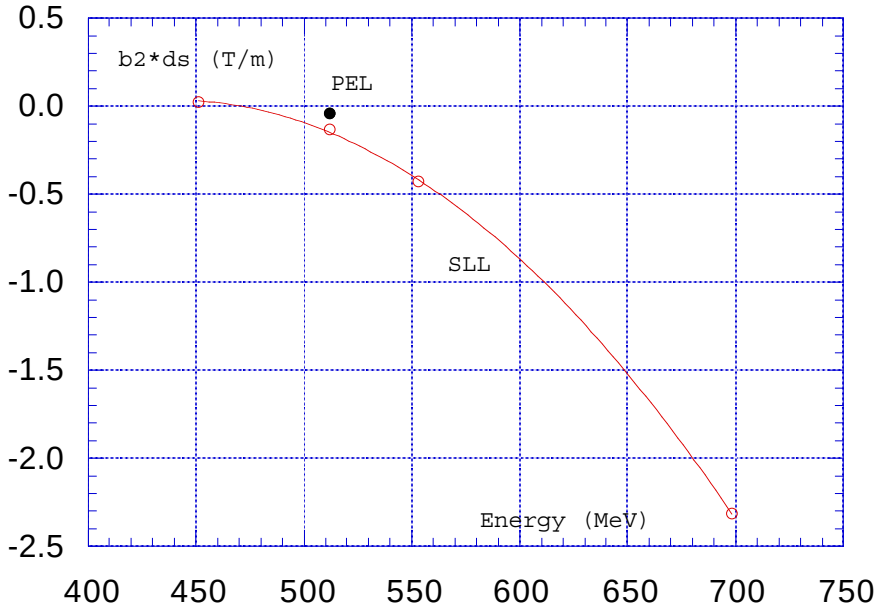

Figure 3.15 - Integrated second order term of the transverse fit versus energy.

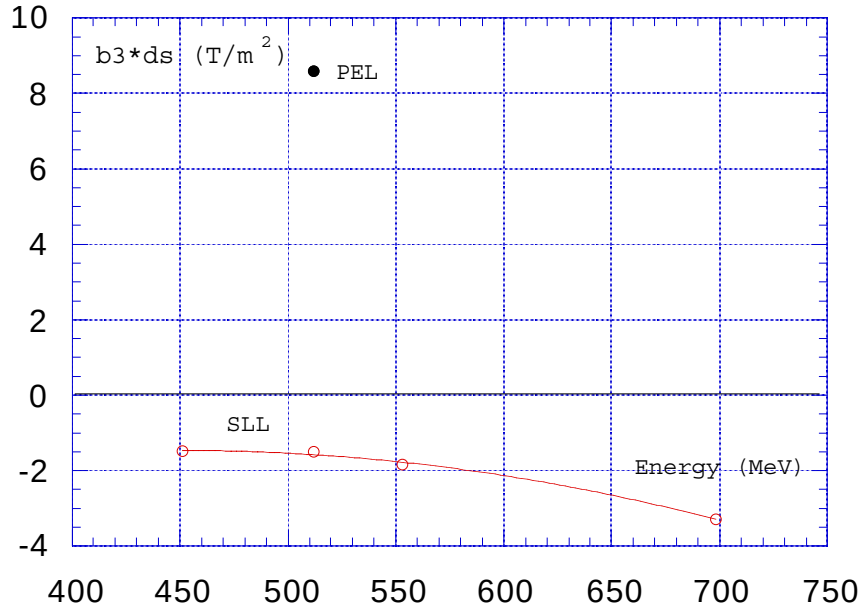

Figure 3.16 - Integrated third order term of the transverse fit versus energy.

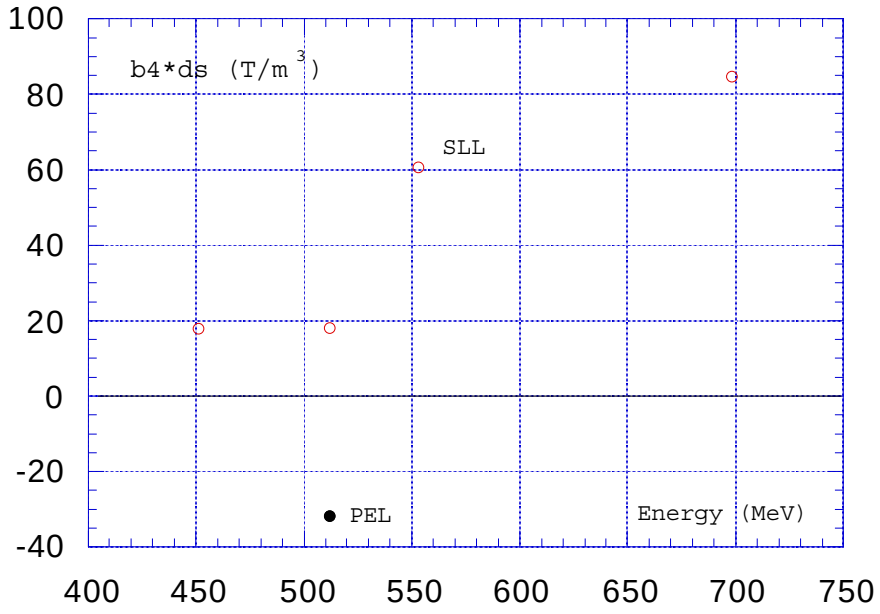

Figure 3.17 - Integrated fourth order term of the transverse fit versus energy.

The last two figures show the dependence on beam energy of the main parameters of the calculated trajectory followed by the particles in the magnets. The maximum distance between the calculated and nominal trajectories in the magnet is given in Fig. 3.18, while Fig. 3.19 shows the difference in length between the two trajectories: both these effects decrease at high beam energy.

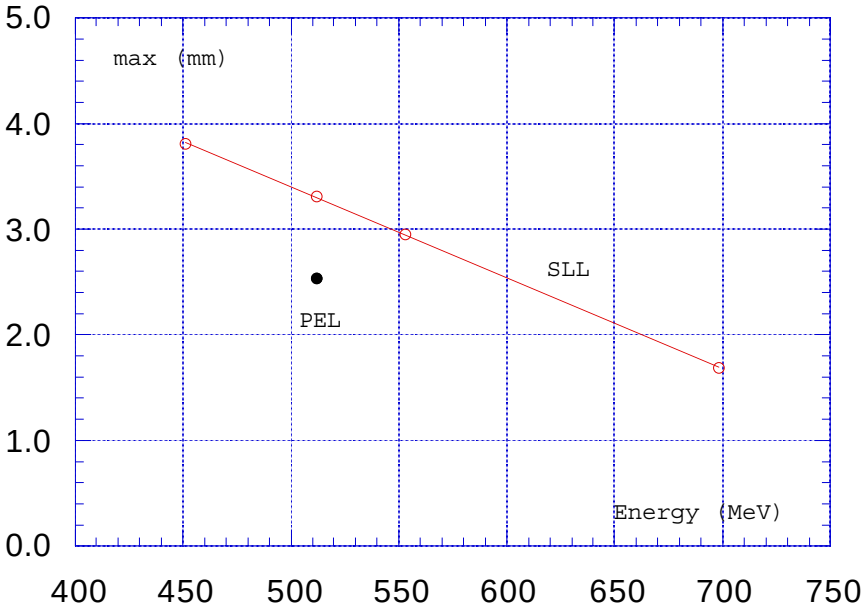

Figure 3.18 - Maximum displacement between real and nominal trajectories versus energy.

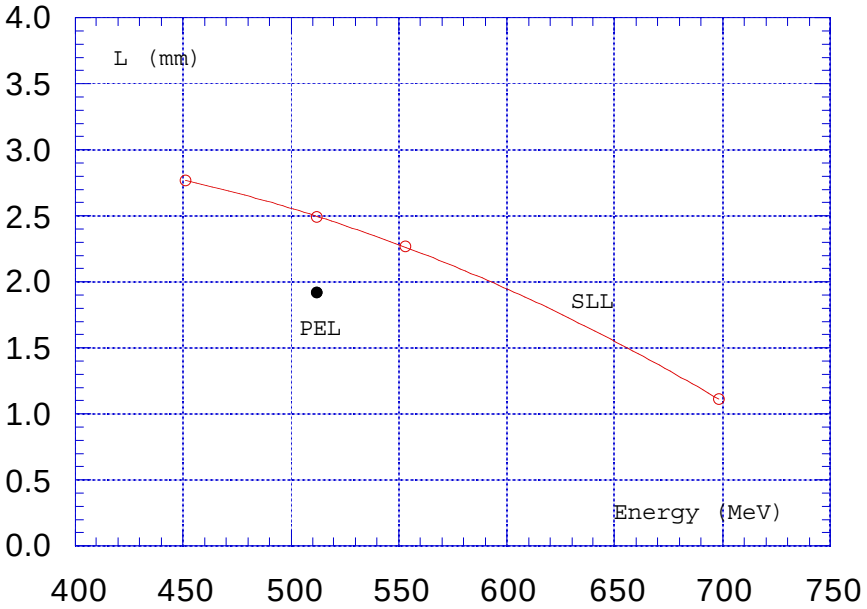

Figure 3.19 - Orbit shortening per magnet versus beam energy.

3.5 - Stray fields

As mentioned before, at large excitation current, the available span of the Hall probe positioning system was not sufficient to measure the stray field of the magnets completely. Figure 3.20 shows the field on the nominal trajectory outside the SLL magnet, namely a straight line at 24.75° with respect to the symmetry axis of the dipole. It can be seen from the figure that at the largest measured current of 502.9 A (well above the nominal operating point at 266.2 A), there is a non negligible negative "overshoot" in the stray field.

The field integrals given above do not take into account the missing part of the field; however, at the distance where it was impossible to measure the field, ≈70 cm from the nominal magnet edge, the field of the magnets in the real machine interferes with those of the neighbouring quadrupoles, so that it is difficult to estimate reliably the effect of the stray fields in the real machine.

Figure 3.21 compares the stray fields of the SLL and PEL dipoles on the nominal operation point.

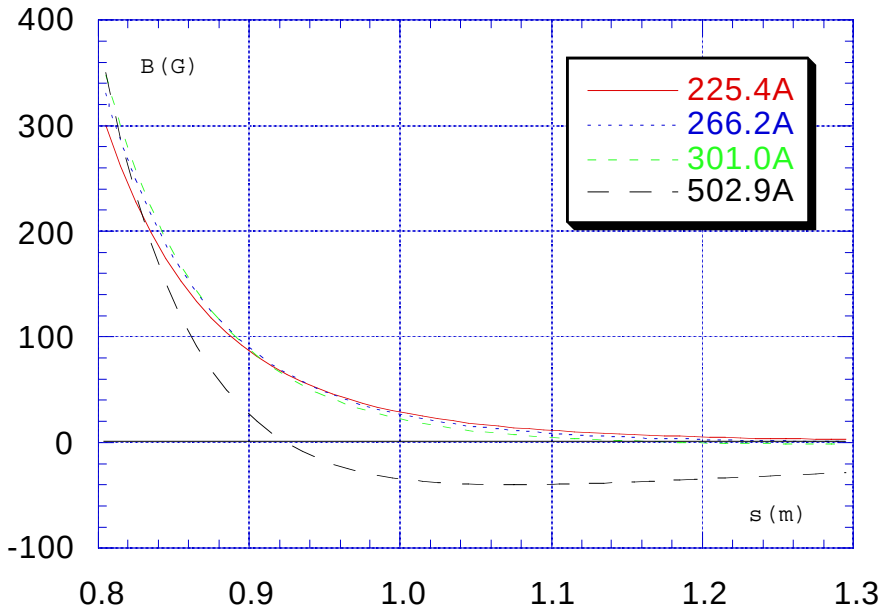

Figure 3.20 - Stray field outside the SLL dipole for different excitation currents. The horizontal coordinate is the distance from the magnet center.

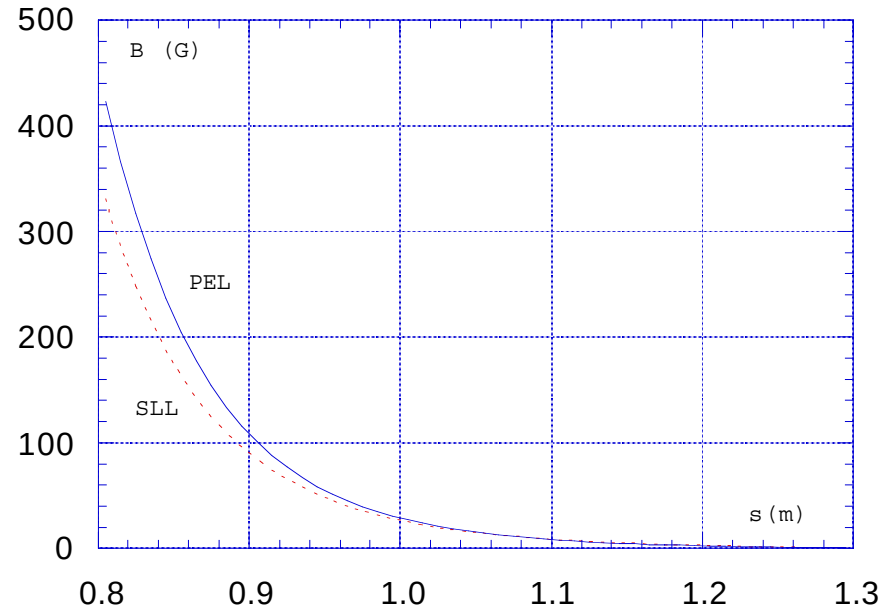

Figure 3.21 - Stray field outside the SLL and PEL dipoles @ 266.2A. The horizontal coordinate is the distance from the magnet center.

A rough measurement of the vertical field component along a horizontal straight line perpendicular to the nominal trajectory of the beam at the magnet center on the side of the iron yoke has been performed for the SLL dipole at the maximum excitation current (≈0.65 kA). We recall that the minimum distance between the beam trajectory in the short section of the other ring and the yoke of the long dipole is ≈1 m.

Figure 3.22 shows the behaviour of the field as a function of the distance from the yoke. The effect on the other beam is negligible at the nominal operating point (≈0.26 kA).

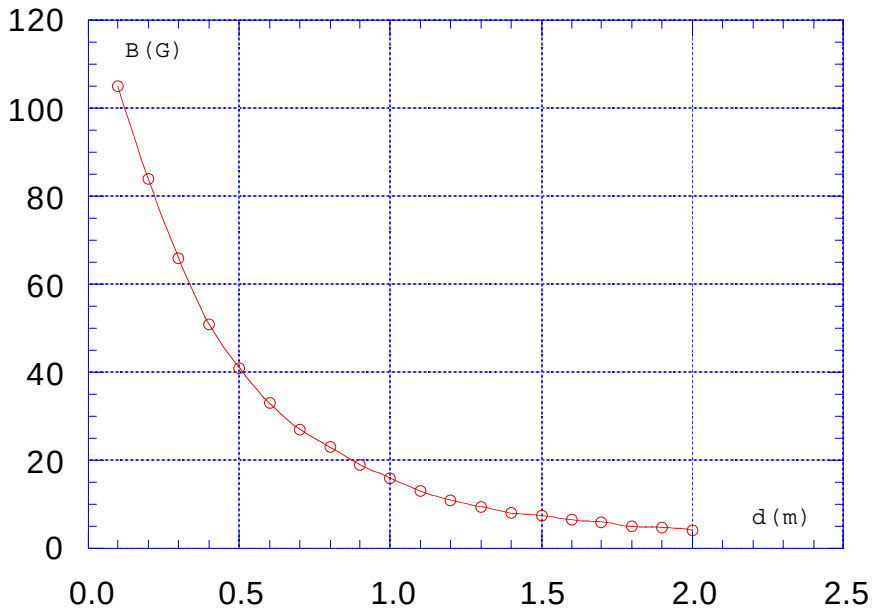

Figure 3.22 - Stray field outside the yoke of the SLL dipole @ 0.65 kA

References

[1] B. Bolli, N. Ganlin, F. Iungo, F. Losciale, M. Modena, M. Paris, M. Preger, C. Sanelli, F. Sardone, F. Sgamma, M. Troiani "The "short" dipoles of the DAΦNE Main Ring achromats" - DAΦNE Technical Note MM-19 (2/8/1996).

[2] B. Bolli, N. Ganlin, F. Iungo, F. Losciale, M. Paris, M. Preger, C. Sanelli, F. Sardone, F. Sgamma, M. Troiani "The dipoles of the DAΦNE Main Ring achromats" - DAΦNE Technical Note MM-26 (to be published).

[3] A. Battisti, B. Bolli, F. Iungo, F. Losciale, M. Paris, M. Preger, C. Sanelli, F. Sardone, F. Sgamma, M. Troiani, S. Vescovi "Measurements and tuning of DAΦNE Accumulator dipoles" - DAΦNE Technical Note MM-9 (29/8/1995).